Synchronization and propagation of bursts in networks of coupled map neurons

Gouhei Tanaka[a)]
Institute of Industrial Science, University of Tokyo, 153-8505, Tokyo, Japan

Borja Ibarz and Miguel A. F. Sanjuan
Nonlinear Dynamics and Chaos Group, Departamento de Matemáticas y Física Aplicadas y Ciencias de la Naturaleza, Universidad Rey Juan Carlos, Tulipán s/n, 28933 Móstoles, Madrid, Spain

Kazuyuki Aihara
Institute of Industrial Science, University of Tokyo, 153-8505, Tokyo, Japan and ERATO Aihara Complexity Modelling Project, JST, 151-0065, Tokyo, Japan

(Received 26 May 2005; accepted 11 November 2005; published online 18 January 2006)

The present paper studies regular and complex spatiotemporal behaviors in networks of coupled map-based bursting oscillators. In-phase and antiphase synchronization of bursts are studied, explaining their underlying mechanisms in order to determine how network parameters separate them. Conditions for emergent bursting in the coupled system are derived from our analysis. In the region of emergence, patterns of chaotic transitions between synchronization and propagation of bursts are found. We show that they consist of transient standing and rotating waves induced by symmetry-breaking bifurcations, and can be viewed as a manifestation of the phenomenon of chaotic itinerancy. © *2006 American Institute of Physics*. [DOI: 10.1063/1.2148387]

Some kinds of neurons are known to exhibit irregular bursting oscillations in response to a constant input current. Network behavior of such bursting neurons has been exhaustively studied, because it may reflect aspects of functional roles in neural assemblies. While these studies usually rely on ordinary differential equation (ODE) neuron models, map-based neurons have been considered as an advantageous alternative for the simulation of large neuronal systems. We use map-based models to study bursting patterns in neural networks. Although regular behaviors such as in-phase and antiphase synchronization of bursts have been replicated in many studies, few have discussed the dynamic mechanism differentiating the two types of burst synchronization in map-based models. Thus, we clarify how the difference between the two synchronous modes lies in local stability of an invariant subspace. The analysis is carried out in such a way that it is valid for a wide variety of network topologies. It also shows that there exist parameter regions where complex spatiotemporal patterns arise in regular, homogeneous networks. Such patterns have received less attention than regular ones, because they are hard to characterize mathematically. Recently, chaotic itinerancy, a concept to deal with complex transient patterns, has been proposed and developed in several case studies. We demonstrate that the complex spatiotemporal patterns found in our model can be characterized as chaotic itinerancy.

I. INTRODUCTION

Synchronization of neuronal burst firings has been intensively studied as a collective behavior possibly related to information transmission and processing in biological neurons. Bursts of spikes, as opposed to single spikes, are considered to enhance the reliability of communications between neurons by facilitating transmitter release.[1] Bursting oscillations are commonly observed in a wide variety of neurons such as hippocampal pyramidal neurons,[2] thalamic neurons,[3] pyloric dilator neurons,[4] in addition to other living cells such as pancreatic beta cells.[5] A useful approach for gaining insight into biological rhythms, such as those produced by central pattern generators,[6] is to elucidate dominant dynamical factors for rhythmic bursting in simple phenomenological models.

In studies on synchronous bursting activities, ordinary differential equation (ODE) neuron models with fast-slow dynamics are most commonly used. Nevertheless, map-based neuron models[7–9] have recently received much attention as reasonable units for simulating collective behaviors in large-scale neural networks.[10] This is because map-based models have been found to be comparable to ODE models in reproducing characteristic behaviors of biological neurons. For instance, synchronization of chaotic bursts has been reproduced by a network of map-based neurons.[7] Two reciprocally coupled map-based neurons[8,11] are able to produce antiphase synchronization of bursts in a similar way to biological neurons[12,13] and ODE models.[14–16] Moreover, transient synchronization encoding temporal activation in coupled inhibitory ODE-based neurons[17] has been reproduced by a similar network of map-based neurons.[18]

In order to further explore the potentials of map-based models, we investigate rhythmic bursting in some networks of 2D map neurons exhibiting chaotic bursts.[7] These networks include rings[19] and lattices,[20] which are amenable to analytic treatment and are used as simple models of neural systems such as the thalamic reticular nucleus and the visual

[a)]Electronic mail: gouhei@sat.t.u-tokyo.ac.jp

cortex.[10,21] Since phenomena of interest in these systems involve generation and propagation of bursting patterns through in-phase and antiphase entrainment and synchronization, we aim in the first place at specifying the dynamic difference between these two synchronization modes. Linear stability analysis reveals how coupling parameters control which synchronous pattern appears. The analysis also shows a parameter region where bursting is emergent, meaning that coupling produces bursting in neurons that would remain silent if isolated.[22,23] In this parameter region, complex spatiotemporal patterns including synchronization and propagation of bursts are observed. We demonstrate that they can be regarded as transitions between chaotic standing and rotating waves[24] induced by destabilization of a fixed point on the invariant subspace of complete synchronization. The transient firing activities are analogous to the chaotic alternations between synchronization and desynchronization found in a network of reduced Hindmarsh-Rose neuron models,[25] and we characterize them as chaotic itinerancy.

Accordingly, the paper is organized as follows. In Sec. II, we introduce the map-based neuron model, and the coupling scheme with chemical and electrical synaptic connections. In Sec. III, we investigate in-phase and antiphase synchronization of bursts in the coupled system and discuss the essential dynamical difference between them. In Sec. IV, we demonstrate how complex transient patterns providing some characteristics of chaotic itinerancy[26] arise in the regular and homogeneous networks. In Sec. V, this study is summarized and related future works are proposed.

II. MODEL

We consider first the following single neuron model proposed by Rulkov:[7,8]

$$x(t+1) = f[x(t)] + y(t), \quad y(t+1) = y(t) - \mu[x(t) - \sigma], \tag{1}$$

where $x(t)$ is the fast variable representing the neuronal membrane potential and $y(t)$ is the slow variable. The difference of the time scales between the two subsystems is determined by a sufficiently small value of the parameter μ, i.e., $0 < \mu \ll 1$. The system of Eqs. (1) can reproduce a variety of neural spiking-bursting activities with a proper nonlinear function f.[7,8] In this study we set $f(x) = \alpha/(1+x^2)$,[7] with a value of α producing chaotic bursts. The parameter σ acts as an external excitation and controls whether the regime of the complete system is silence, bursting, or tonic spiking.

To understand the behavior of the model, we consider the dynamics of the 1D fast subsystem given as follows:

$$x(t+1) = f[x(t)] + y, \tag{2}$$

where y works now as a parameter. As y is varied, the return map of Eq. (2) shifts vertically. For this variation, the fast subsystem shows hysteresis between a steady state and an oscillatory state, giving rise to bursting behaviors. A typical orbit showing irregular bursting is depicted by bold curves in Fig. 1(a). The gray branches indicate the stable and unstable fixed points, which coalesce via the saddle-node (fold) bifurcation at $y = y_{sn}$ with increasing y. The gray region in Fig. 1(a) indicates the chaotic attractors, which disappear through the (homoclinic type) boundary crisis at $y = y_{cr}$ with decreasing y. Hence, the 2D map is classified as a "fold/homoclinic"-type bursting model according to the bifurcations of the 1D fast submap.[9] Three different regimes can be reproduced depending on the value of the control parameter σ. When the line $x = \sigma$ intersects the branch of the stable fixed points, the intersection point (unless it is very near the fold) is a stable fixed point corresponding to the silence regime in the complete system. When the line $x = \sigma$ is set between the ranges of the two quasiattracting states, $y(t)$ increases if $x(t) < \sigma$ and decreases otherwise. As a result, an orbit in the complete system exhibits repetitive transitions between the silence and bursting phases as shown in Fig. 1(a). The corresponding time series of the fast and slow variables are shown in Fig. 1(b). When σ is sufficiently large, a typical orbit sustains a chaotic oscillation corresponding to the regime of tonic spiking.

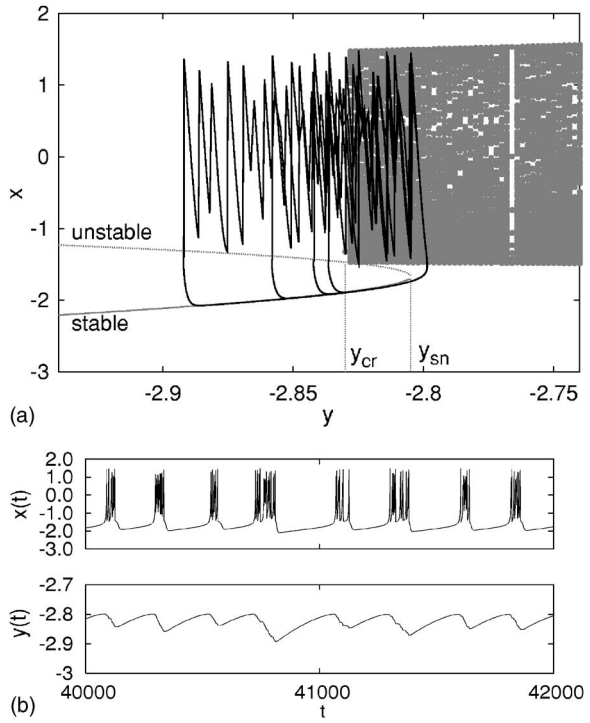

FIG. 1. (a) Phase portrait of a typical bursting behavior (black) in the Rulkov model (Ref. 7) computed with $\alpha = 4.3$, $\sigma = -1.5$, and $\mu = 0.001$. The discrete orbit points are connected in the order of time steps. It is superimposed on the bifurcation diagram (gray) of the fast subsystem, where the gray branches indicate the stable and unstable fixed points merging at the saddle-node bifurcation point (y_{sn}) and the gray region represents the chaotic attractors vanishing at the boundary crisis point (y_{cr}). The bursting motion in the total system is due to hysteresis between the two states in the fast subsystem. (b) Time series of the fast and slow variables in a bursting regime.

In the complete 2D system of Eqs. (1), the transition from a steady state to a bursting state corresponds to a subcritical Neimark-Sacker bifurcation of a stable fixed point, which is closely related to a saddle-node bifurcation in the fast subsystem. Figure 2(a) shows the phase diagram of the model in the (σ, α) parameter plane. The boundary separating the silence and bursting regimes is given by the Neimark-Sacker bifurcation curve, which lies in the vicinity

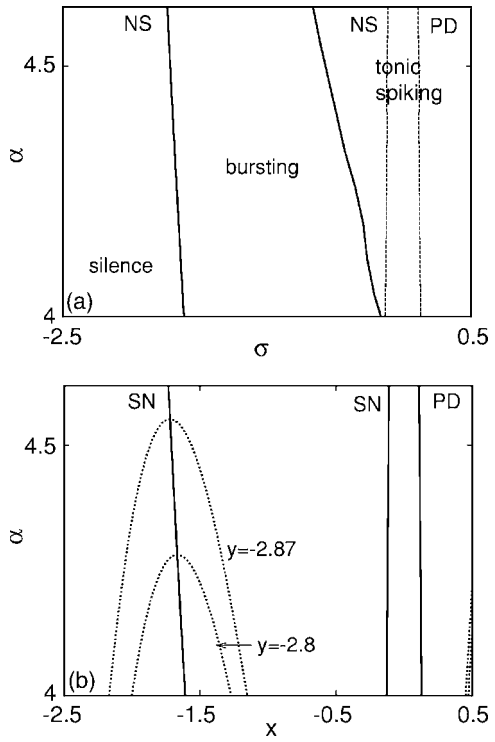

FIG. 2. (a) Phase diagram of the Rulkov model (Ref. 7) including the silence, bursting, and tonic spiking regimes. The boundary separating the silence and bursting regimes is given by the Neimark-Sacker (NS) bifurcation curve. The other Neimark-Sacker bifurcation and the period-doubling (PD) bifurcation curves are also depicted by the dashed lines. (b) The sets of points specified by (x,α) at the saddle-node (SN) and period-doubling (PD) bifurcation points as y is varied in the fast subsystem of the Rulkov model. The dashed curves indicate the branches of fixed points at fixed values of y.

of the set of saddle-node bifurcation points in the fast subsystem as shown in Fig. 2(b). On the other hand, the boundary separating the regimes of bursting and tonic spiking in Fig. 2(a) is roughly drawn, because it is not characterized by a local bifurcation.

Next we introduce the network model of N identical neurons represented by the following equations:

$$\begin{aligned} x_n(t+1) &= f[x_n(t)] + y_n(t) - g_c h_n^c(t) + g_e h_n^e(t), \\ y_n(t+1) &= y_n(t) - \mu[x_n(t) - \sigma], \quad n = 1, \ldots N, \end{aligned} \tag{3}$$

where chemical and electrical synapses are simply modeled as follows:

$$h_n^c(t) = \sum_1^N \gamma_{nm}^c [x_m(t) - \nu], \tag{4}$$

$$h_n^e(t) = \sum_1^N \gamma_{nm}^e [x_m(t) - x_n(t)]. \tag{5}$$

In these equations, the fast and slow variables of the nth neuron are represented by x_n and y_n, respectively. We consider chemical synapses to be inhibitory with $g_c \geqslant 0$, and electrical coupling to be diffusive with $g_e \geqslant 0$, obtaining a minimal configuration based on previous studies.[8,11,18] Coefficients γ_{nm}^c and γ_{nm}^e take values of 1 or 0 depending on whether or not there exists chemical and electrical coupling, respectively, between neurons n and m. We study networks where chemical and electric couplings are combined, meaning that electrical synapses are accompanied by chemical synapses; therefore, all chemical synapses are assumed to be formed with neighbors like electrical synapses. This assumption greatly simplifies the analytic treatment of the problem.

With this configuration, burst firing of a neuron induces a current which reduces the potentials of the postsynaptic neurons through the inhibitory chemical coupling. It should be noted that the chemical coupling term is negligible during a resting phase because the threshold value ν is assumed to be close to the level of the resting potential. The difference of potentials between connected neurons also generates a current flow injected from a neuron with a high voltage into a neuron with a low voltage through the diffusive electrical coupling. This modeling of coupling is analogous to that usually found in ODE-based systems and enables the map-based model to reproduce similar network behaviors. This is because the map-based model is derived from an ODE-based model by a difference scheme such as the Euler method, rather than a reduction method with Poincaré sections.

In the rest of the paper, the Rulkov model and the coupling scheme we have presented are used with the following parameter values: $\alpha=4.3$, $\nu=-2.5$, and $\mu=0.001$.

III. LINEAR ANALYSIS OF BURSTING

In this section we investigate the mechanism that gives rise to in-phase and antiphase bursting patterns in networks of map-based neurons, and how network parameters separate these two regimes. The analysis performed also specifies the parameter region where bursting appears as an emergent property of the network.[23] In this region we observe complex, aperiodic activity patterns similar to those found in real networks, even though our models are perfectly regular and homogeneous. Such patterns will be investigated in the next section.

Figures 3 and 4 illustrate the two fundamental modes of synchronization that lie in the basis of more complex patterns. Figure 3 shows the in-phase synchronization of bursts in a ring of 32 map neurons coupled with $g_c=0$ and $g_e>0$. Synchronization arises due to entrainment by the diffusive coupling term in Eqs. (3): if the nth neuron is at rest and one of its two neighbors begins bursting, the additive term of the fast subsystem of the nth neuron increases largely and its orbit may cross over the branch of unstable fixed points. Hence, a neuron which fires a burst triggers the onset of bursting of its neighbor neurons. The avalanche of synchronous switching yields the synchronized chaotic bursts.[7] Burst synchronization indicates a coincidence of the beginning and the end of each burst,[12] while spikes inside each burst need not be synchronized.

If coupling parameters are $g_c>0$ and $g_e=0$ instead, the antiphase synchronization shown in Fig. 4 results. In this case, the fast subsystem of the nth neuron is subtractively affected by its two neighbors through the inhibitory coupling in Eqs. (3). If any of the neighbors of the nth neuron begins bursting, the nth neuron is pushed to its resting state, because a significantly negative value of the coupling term forces its orbit to cross the branch of the stable fixed points in the fast

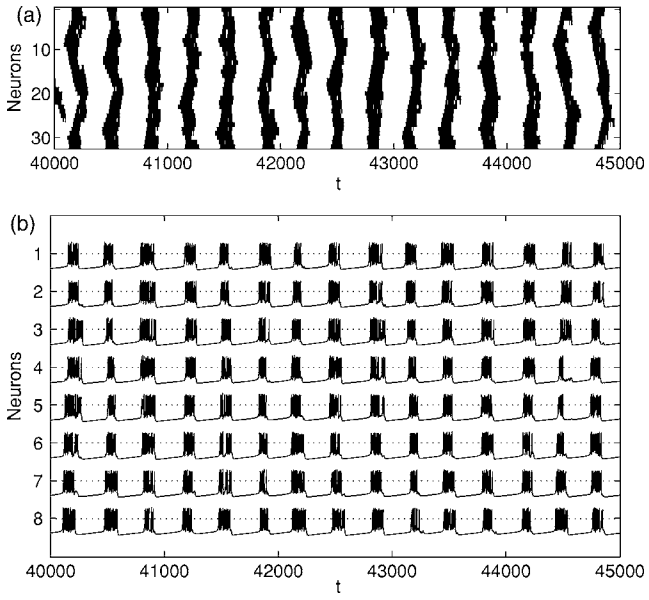

FIG. 3. In-phase synchronization of bursts computed in a ring with $N=32$, $\sigma=-1.5$, $g_c=0$, and $g_e=0.05$. (a) Spatiotemporal patterns in a raster plot. The bursting and resting phases are indicated by black and white, respectively. (b) Time series of the fast variables of 8 neurons in the network.

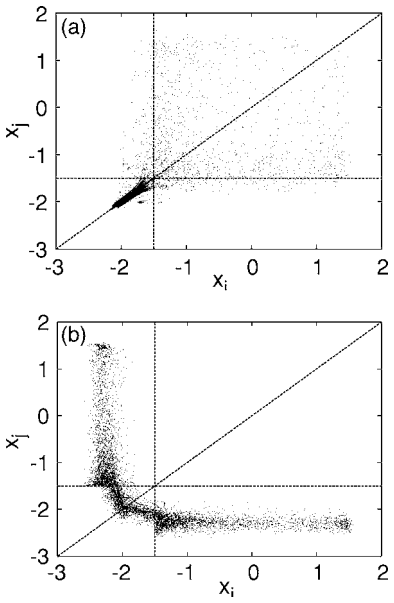

FIG. 5. Projections of orbits of the synchronized bursts in the ring network. (a) An orbit moves along the diagonal during a resting phase in the in-phase case where $g_c=0$ and $g_e=0.05$. A similar picture is observed for any two fast variables (x_i,x_j) where $i\neq j$; (b) An orbit exhibits transitions between the two out-of-diagonal states in the antiphase case where $g_c=0.05$ and $g_e=0$. A similar picture is observed for fast variables of any two neighbor neurons (x_i,x_j) where $|i-j|=1$.

subsystem. When the neighbors switch to a resting state, the nth neuron is driven to a bursting state due to a large increase in the coupling term. Hence, any two neighbor neurons always take different phases and fire bursts alternately.

The difference of orbital motions between these two synchronous patterns can be confirmed in the projections of the orbits illustrated in Fig. 5. The vertical and horizontal dashed lines, indicating $x_i=\sigma$ and $x_j=\sigma$, roughly separate the projection plane into four regions according to whether each neuron is resting or bursting. In the regime of in-phase synchronization, the fast variables of any two neurons are almost identical when at rest, while they seem to be uncorrelated during a bursting phase as shown in Fig. 5(a). A typical orbit moves during a resting phase along the two-dimensional invariant subspace Π where $x_1=x_2=\cdots=x_N$ and $y_1=y_2=\cdots=y_N$, corresponding to the diagonal in the projection picture. It should be noted that 2^N states are potentially quasiattracting because of the bistability of each fast subsystem. Conversely, in the regime of antiphase synchronization a neuron is bursting while its neighbors are resting and vice versa, as shown in Fig. 5(b). In this regime, orbits near Π are repelled transversely, exhibiting transitions between the two states away from the invariant subspace. Therefore, it is the local stability of Π, influenced by the coupling parameters, that decides which of the two different regimes will emerge.

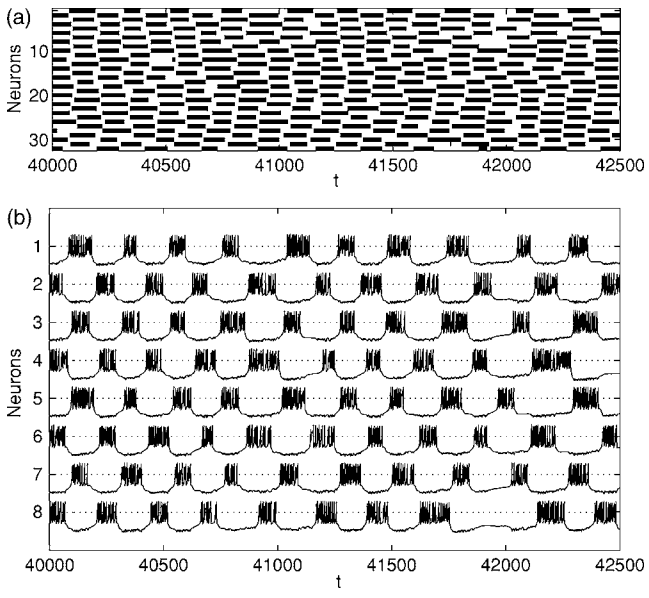

FIG. 4. Alternating rhythmic bursting computed in a ring with $N=32$, $\sigma=-1.5$, $g_c=0.05$, and $g_e=0$. (a) Spatiotemporal patterns in a raster plot. The bursting and resting phases are indicated by black and white, respectively. (b) Time series of the fast variables of 8 neurons in the network.

We now formalize and extend the previous intuitive analysis by investigating the stability of the invariant subspace Π with the help of master stability functions.[27] The Jacobian matrix of Eqs. (3) at a point on Π where $x_i=r$ for $1\leqslant i\leqslant N$ can be written in the following compact form:

$$J=I_N\otimes F+G\otimes H, \tag{6}$$

where I_N is the $N\times N$ identity matrix,

$$H=\begin{pmatrix}1 & 0\\ 0 & 0\end{pmatrix},\quad F=\begin{pmatrix}f'(r) & 1\\ -\mu & 1\end{pmatrix},$$

and $G=-g_c\Gamma_c+g_e\Gamma_e$, Γ_c and Γ_e being the adjacency matrices of the graphs of chemical and electric connections

$$\Gamma_c = \begin{pmatrix} 0 & \gamma^c_{12} & \cdots & \gamma^c_{1N} \\ \gamma^c_{21} & 0 & \cdots & \gamma^c_{2N} \\ \vdots & & \ddots & \vdots \\ \gamma^c_{N1} & \gamma^c_{N2} & \cdots & 0 \end{pmatrix},$$

$$\Gamma_e = \begin{pmatrix} -\sum_{i\neq 1} \gamma^e_{1i} & \gamma^e_{12} & \cdots & \gamma^e_{1N} \\ \gamma^e_{21} & -\sum_{i\neq 2} \gamma^e_{2i} & \cdots & \gamma^e_{2N} \\ \vdots & & \ddots & \vdots \\ \gamma^e_{N1} & \gamma^e_{N2} & \cdots & -\sum_{i\neq N} \gamma^e_{Ni} \end{pmatrix}.$$

Now, since all neurons are identical in Π, the matrix F is the same for all of them, $I_N \otimes F$ is block identical, and diagonalization of the Jacobian J is achieved by simply diagonalizing the connectivity matrix G. We obtain then a block diagonal matrix, with each block (2×2) given as follows:

$$M_k = F + s_k H, \quad k = 0, \ldots, N-1, \tag{7}$$

where s_k are the eigenvalues of G. In this way the influence of the network topology on stability is clearly separated from that of the intrinsic neuron dynamics. In the case of a ring, G is a circulant matrix; its eigenvalues are easily obtained as

$$s_k = -2(g_e - \delta \cos k\theta), \tag{8}$$

where $\theta = 2\pi/N$ and $\delta = g_e - g_c$. All eigenvalues are therefore in the interval between $-2(g_e-\delta)$ and $-2(g_e+\delta)$. If the network is a lattice with a 4-neighborhood as the product of two rings, eigenvalues s_k of G similarly spread in the interval between $-4(g_e-\delta)$ and $-4(g_e+\delta)$. In any case, by restricting ourselves to symmetric coupling, all s_k are real.

The eigenvalues of the complete system are now obtained from each block in Eq. (7) as follows:

$$\lambda_{k\pm}(r) = \frac{f'(r) + 1 + s_k \pm \sqrt{(f'(r) - 1 + s_k)^2 - 4\mu}}{2}. \tag{9}$$

If $|\lambda_{k\pm}(r)| < 1$ for all k, the invariant subspace Π is stable around $x_i = r$, $i = 1, \ldots, N$. Otherwise, the behavior near Π is dominated by the eigenvectors corresponding to the $\lambda_{k\pm}$ with the maximum absolute value.

A contour plot of the maximum absolute values of the eigenvalues $\lambda_{k\pm}$ as a function of r and s_k in logarithmic scale is useful to visualize these features. Such plot is universal in the sense that it is completely determined by the neuron model. For any network topology we only have to position the points corresponding to the eigenvalues s_k of G [e.g., those given in Eq. (8) in the case of a ring] and the value of r under study, to see which modes are unstable to what degree and how stability depends on coupling parameters.

Figure 6 shows this kind of plot for the particular case of a ring of 6 neurons, in two different cases with $\delta > 0$ and $\delta < 0$. The solid contour is the boundary of stability; points to the right of this curve have eigenvalues of modulus greater than 1 for the complete system. For any given r, the eigenvalues s_k of G given by Eq. (8) are distributed along the horizontal segment with endpoints at $-2(g_e \pm \delta)$. In other networks with symmetric matrix G, eigenvalues would be similarly distributed along a different segment. In all cases, the rightmost point in the segment will have the largest eigenvalue and therefore will be the dominant mode near Π. Thus, in Fig. 6(a) where $\delta > 0$, the rightmost mode corresponds to s_0, whose eigenvector V_0 is parallel to Π. Whenever this mode lies in the unstable region as in the case of $r = -1.6$, a typical orbit near the invariant subspace Π is repelled in the direction tangent to Π. Therefore, the presence of a reinjection mechanism into the vicinity of Π forces orbits to iterate transitions between the bottom-left region and the upper-right region on the projection plane as shown in Fig. 5(a). On the other hand, in Fig. 6(b) where $\delta < 0$, the rightmost dominant mode corresponds to s_3, whose eigenvector V_3 is perpendicular to Π. Thus, whenever this mode lies in the unstable region as in the case $r = -1.6$, an orbit with a small perturbation apart from Π is repelled in the direction transverse to Π. Therefore, the absence of a reinjection mechanism into Π leads to the rapid transitions between the

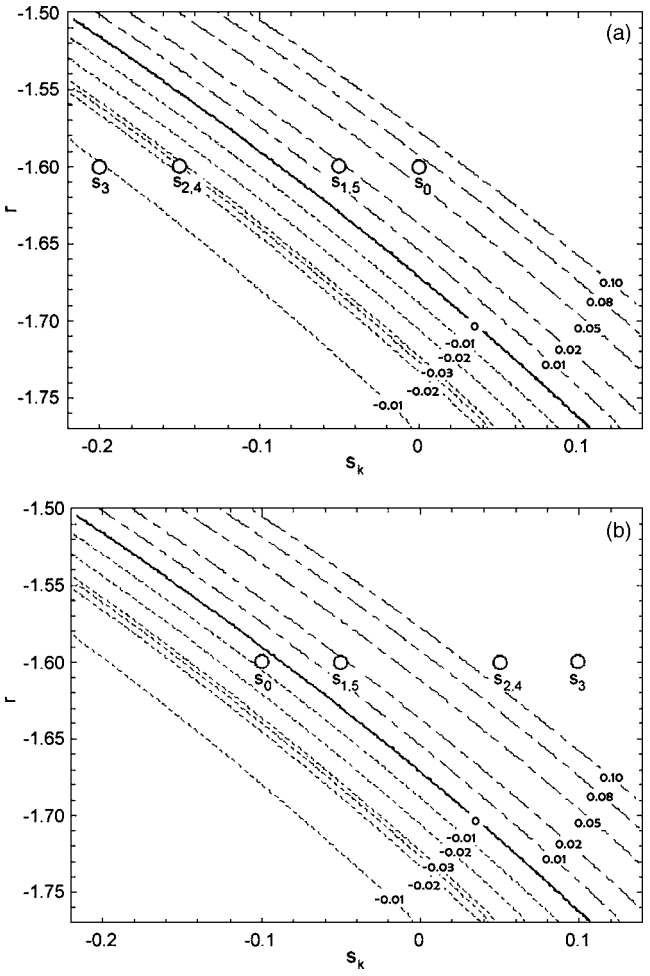

FIG. 6. Contours of constant logarithm of the modulus of the maximum eigenvalue of the complete system at the invariant subspace Π as a function of r and the eigenvalues of the connectivity matrix, s_k. The solid line is the boundary of stability. Circles represent eigenvalues of the connectivity matrix for a ring of $N=6$ neurons; the eigenvector of mode s_0 is parallel to Π, while that of mode s_3 is transverse to it and corresponds to a π phase shift between neighbor neurons. (a) $\delta > 0$ with $g_c = 0$ and $g_e = 0.05$. (b) $\delta < 0$ with $g_c = 0.05$ and $g_e = 0$.

bottom-right region and the upper-left region on the projection plane, as shown in Fig. 5(b).

The previous discussion is valid for any ring or lattice, or indeed for any regular network with combined electric and chemical connections such that $\Gamma_e=\Gamma_c-dI_N$, where d is the degree of the network. Whenever $\delta>0$, the dominant eigenvalue corresponds to the unique eigenvector parallel to Π and produces in-phase synchronization, while with $\delta<0$ dominant eigenmodes are transverse to Π and produce alternating burst patterns whose complexity depends on the dimension of the corresponding eigenspace.

Whether these bursts develop into a homogeneous state of the whole network or give rise to traveling patterns depends on global characteristics of the system. Patterns are particularly interesting in the emergence region,[23] where bursting appears for values of σ where isolated neurons would remain silent. The following analysis allows us to determine the emergence region. For the whole network to be silent, the unique fixed point of Eqs. (3), satisfying

$$x_1=x_2=\cdots=x_N=\sigma, \tag{10}$$

$$y_1=y_2=\cdots=y_N=\sigma-f(\sigma)+dg_c(\sigma-\nu), \tag{11}$$

must be stable, that is, in the master stability diagram all the s_k must lie to the left of the stability boundary when $r=\sigma$. In the case of isolated neurons, $s_k=0$ for all k. Therefore, the necessary and sufficient condition for emergent bursting is that some $s_k>0$, which is equivalent to $\delta<0$ in the networks we study. The lower δ, the broader the emergence region for σ. In the case of a ring, where we have simple analytic expressions for the s_k in Eq. (8), the boundary of emergent bursting that corresponds to the subcritical Neimark-Sacker bifurcation of the stable fixed point turns out to be given for $\delta<0$ as follows:

$$\alpha=-(1-\mu-s_{[N/2]})(1+\sigma^2)^2/2\sigma. \tag{12}$$

The dependence of this boundary on coupling parameters and the number of neurons in the ring is shown in Fig. 7. For fixed g_e and N, the emergence region becomes larger with increase of g_c as expected and shown in Fig. 7(a). The number of neurons influences the size of the emergence region because $s_{[N/2]}=2(g_c-2g_e)$ for even N while $s_{[N/2]}=2[(g_c-g_e)\cos(\theta/2)-g_e]$ for odd N. Thus, for fixed g_c and g_e, the size of the emergence region is constant for even N, while for odd N it approaches the constant value in the case of even N with increasing N as shown in Fig. 7(b).

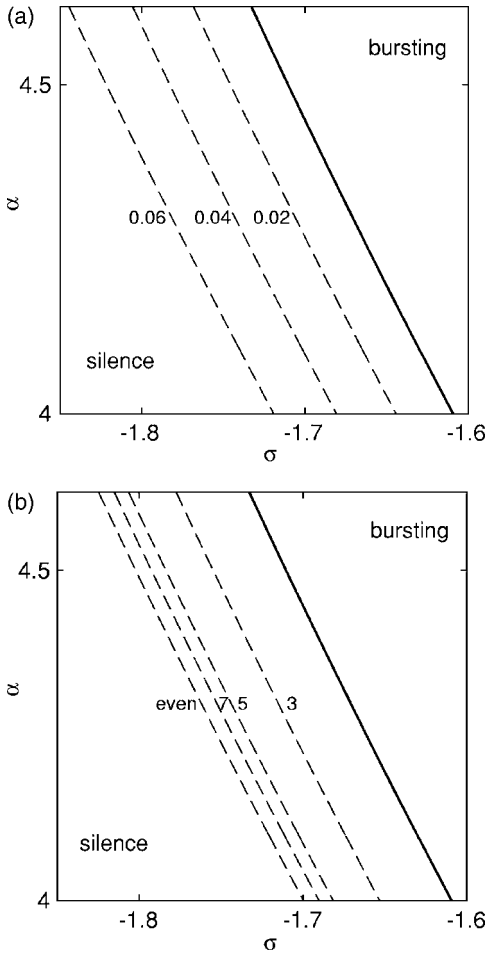

FIG. 7. (a) Effect of the coupling parameters on the size of the emergence region in a ring. The solid line indicates the boundary for uncoupled neurons. The dashed lines indicate the boundaries for different values of g_c, where $g_e=0$ and N is even. (b) Effect of the number of neurons for the size of the emergence region. The dashed lines indicate the boundaries for different values of N, where $g_c=0.05$ and $g_e=0$.

IV. COMPLEX PATTERNS AS CHAOTIC ITINERANCY

Possible roles of chaos in the brain have been discussed with the aid of some concepts of nonlinear dynamics to obtain a picture of dynamical and adaptive information processing by neuronal populations.[28] Among these concepts, chaotic itinerancy, which describes chaotic transitions of a trajectory among nearly ordered motions around Milnor's attractors,[26] has been proposed as a mechanism for memory association, with each ordered motion corresponding to a memory and the itinerant transitions representing their dynamical associations. This contrasts with the similar concept of winnerless competition, where information is retrieved not from the attractors themselves but from the movement along heteroclinic orbits dependent on input stimuli[17] giving rise to sequential switching among the different equilibria.

Characterization of chaotic itinerancy in a network of coupled ODE-based neuron models has been done recently[25] with the analysis of a collective pattern consisting of chaotic alternations between synchronized and desynchronized states. This transient motion can be responsible for dynamic changes of functional roles in cell assemblies. It has been suggested that the spatiotemporal activity of neural assemblies at the mesoscopic level may be responsible for higher-level functions such as memory, perception, and cognition. A similar analysis of transient activities is performed in this section in the networks of map-based models represented by Eqs. (3), and, although no precise mathematical definition of the concept has been agreed upon yet, we show that dynamic properties such as convergence of Lyapunov exponents and persistence of correlations point towards chaotic itinerancy.

We consider network dynamics in the parameter range of emergent bursting already discussed. We concentrate on a ring network, where propagation of bursts is most easily

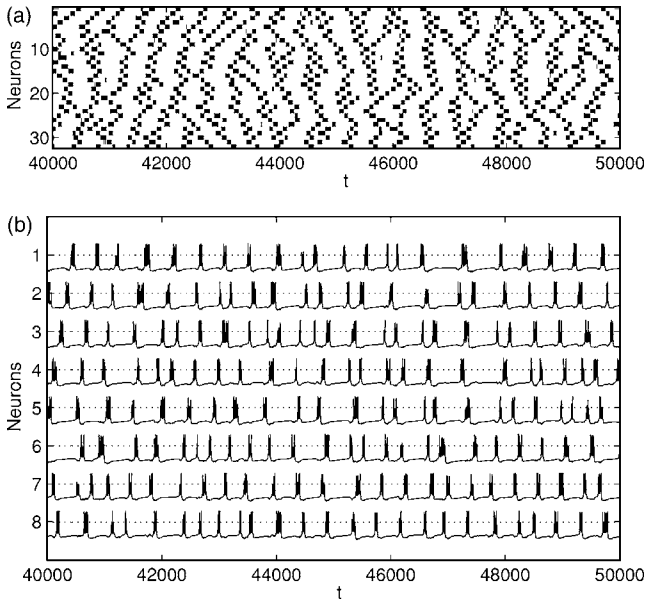

FIG. 8. Complex patterns including propagations of bursts in a ring computed with $N=32$, $\sigma=-1.65$, $g_c=0.02$, and $g_e=0$. (a) Spatiotemporal patterns in a raster plot. The bursting and resting phases are indicated by black and white, respectively. (b) Time series of the fast variables of 8 neurons in the network.

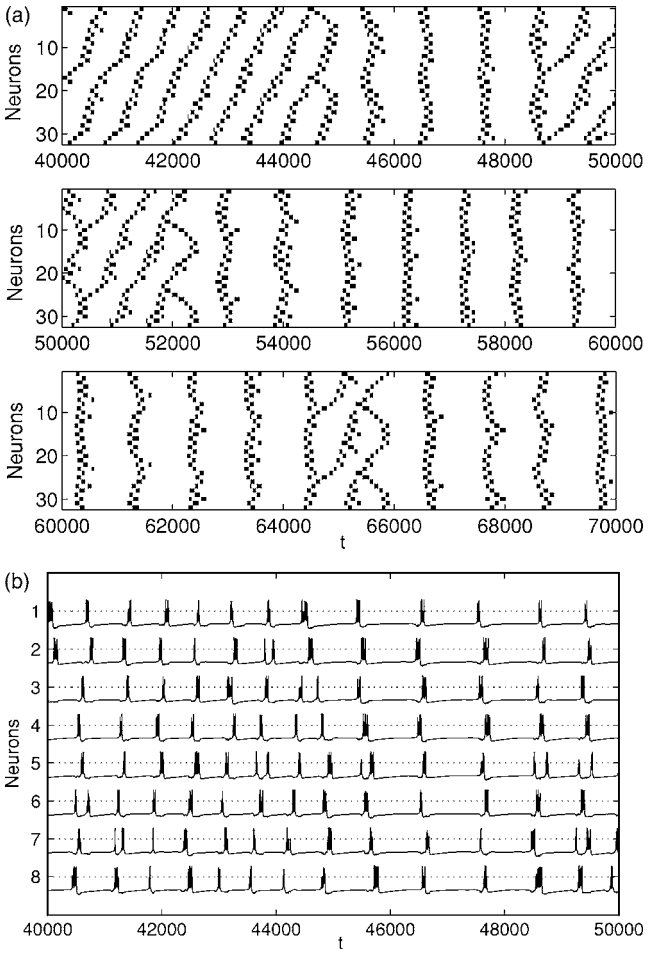

FIG. 9. Complex pattern consisting of transitions between synchronous and propagating bursts in a ring computed with $N=32$, $\sigma=-1.69$, $g_c=0.02$, and $g_e=0$. (a) Spatiotemporal patterns in a raster plot. The bursting and resting phases are indicated by black and white, respectively. (b) Time series of fast variables of 8 neurons in the network.

characterized; similar phenomena appear in the emergence region of lattices. We change the value of the parameter σ, fixing the coupling at $g_c=0.02$ and $g_e=0$ with $\delta<0$. Alternating rhythmic bursting is observed at $\sigma=-1.6$ as shown in the previous section. As σ is decreased, the alternating rhythm is gradually lost and instead a complex pattern sets in as shown in Fig. 8. Figure 8(a) shows that the resting phases are predominant over the bursting phases; the average bursting rate declines with decreasing σ. The network behavior appears rather irregular temporally, as can be appreciated by the variety of interval lengths between two consecutive bursts. Nevertheless, it seems to include local spatiotemporal characteristics such as propagations of bursts as shown in Fig. 8(b). Further decrease of σ results in a pattern consisting of irregular transitions between nearly synchronous and propagating bursts as shown in Fig. 9(a). The synchronized long plateaus stem from slow motion of an orbit in the vicinity of the invariant subspace Π. Figure 9(b) clearly illustrates a transition from a regime of propagating bursts to a regime of synchronous bursts. The interval length between two consecutive synchronized bursts roughly grows as σ approaches the bifurcation point beyond which the network turns silent.

The symmetry of the ring plays a key role in understanding the complex spatiotemporal patterns. According to the studies on rings of coupled identical oscillators,[29,30] standing and rotating waves are typically induced by destabilization of a steady state on the synchronization manifold. Several branches of solutions are generated by a degenerated Hopf bifurcation due to symmetry breaking. It should be noted that this property originates from the network configuration regardless of the dynamics of individual oscillators. Although the instability of the steady state is induced by a Neimark-Sacker bifurcation of a fixed point in our case, several branches of solutions are still expected to emerge from the singular point. Figure 10 illustrates transient behaviors corresponding to chaotic standing and rotating waves. Figure 10(a) shows a transversally unstable solution confined in the four-dimensional invariant subspace where $(x_1,y_1)=(x_3,y_3)=\cdots=(x_{N-1},y_{N-1})$ and $(x_2,y_2)=(x_4,y_4)=\cdots=(x_N,y_N)$. This pattern suggests that chaotic standing waves as shown in Fig. 10(b) can be understood as iterations of escape from and entry into nearly synchronized resting phases. Figures 10(c) and 10(d) illustrate clockwise and anticlockwise propagations of bursts corresponding to chaotic rotating waves. Furthermore, those corresponding to fast rotating waves can also be found as shown in Figs. 10(e) and 10(f). In this way, a complex pattern as shown in Figs. 8 and 9 can be viewed as switching over several modes of waves such as those exemplified above.

In order to characterize the change of the complex spatiotemporal patterns with variation of σ, we investigate the degree of orbital instability by estimating the Lyapunov exponents. The Lyapunov exponents can be calculated by considering expanding and contracting rates in each direction of orthonormal vectors along the time evolution of orbits. Figure 11 shows the variation of the Lyapunov dimension D_L

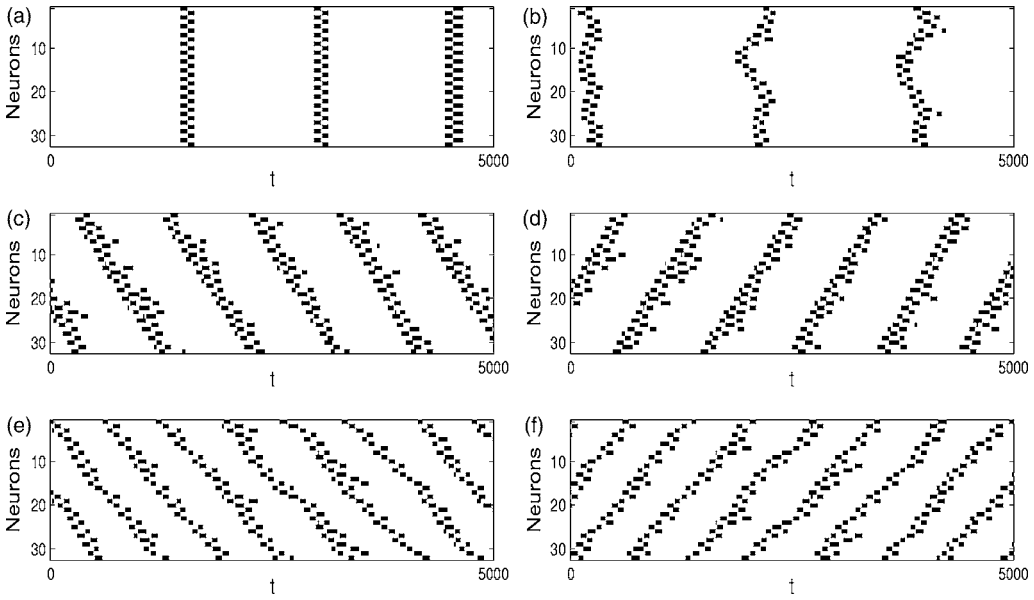

FIG. 10. Examples of transient ordered motions found in a ring where $N=32$, $\sigma=-1.69$, $g_c=0.02$, and $g_e=0$: (a) a solution with synchronized resting states in a four-dimensional invariant subspace; (b) nearly synchronized bursts corresponding to standing waves; (c) and (d) propagating bursts corresponding to (c) clockwise and (d) counterclockwise rotating waves; (e) and (f) propagating bursts corresponding to (e) clockwise and (f) counterclockwise fast rotating waves.

indicating the effective dimension of an attractor and the topological dimension D_T. For a system with Lyapunov exponents $\lambda_i (i=1,2,\ldots)$, the Lyapunov dimension is defined as $D_L=j+\Sigma_{i=1}^{j}\lambda_i/|\lambda_j|$ where $\lambda_i \geqslant \lambda_{i+1}$ for all i, and j is the integer such that $\Sigma_{i=1}^{j}\lambda_i \geqslant 0$ and $\Sigma_{i=1}^{j+1}\lambda_i < 0$.[31] The topological dimension D_T is given as the number of non-negative Lyapunov exponents. Hence, the dimension gap between D_L and D_T approximately represents the number of negative exponents with very small absolute values. The dimension gap is large because the slow dynamics is neither expanding nor contracting. The declining dimensions with decrease of σ imply that the average bursting rate falls with the prominence of lower-dimensional states where the number of simultaneously bursting neurons is relatively small.

Figure 12 shows time evolutions of the computation of the largest Lyapunov exponent for different values of σ. The slow convergence implies that an orbit exhibits transitions among states with various dimensions. The network of coupled bursting neurons has 2^N quasiattracting states according to whether each neuron is bursting or resting. In fact, they include a wide variety of motions from a low-dimensional ordered motion such as a synchronized resting state to a highly developed chaotic motion such as a synchronized bursting state. The convergence of the largest Lyapunov exponent becomes slower as σ approaches the transition point to the silence regime. We also calculate the autocorrelation and the cross correlation of the time evolution of the x components as shown in Figs. 13(a) and 13(b).

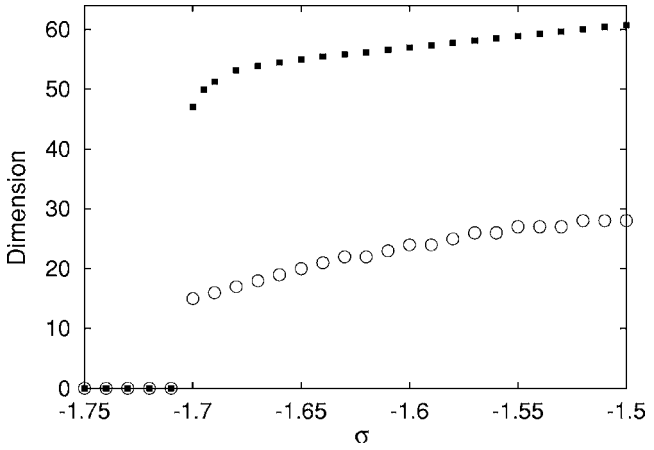

FIG. 11. Variation of the Lyapunov dimension D_L (filled box) and the topological dimension D_T (open circle) with change of σ where $N=32$, $g_c=0.02$, and $g_e=0$. The large number of dimension gap given by D_L-D_T implies that an attractor is distributed over a wide range in phase space. Both dimensions are zero for the steady state.

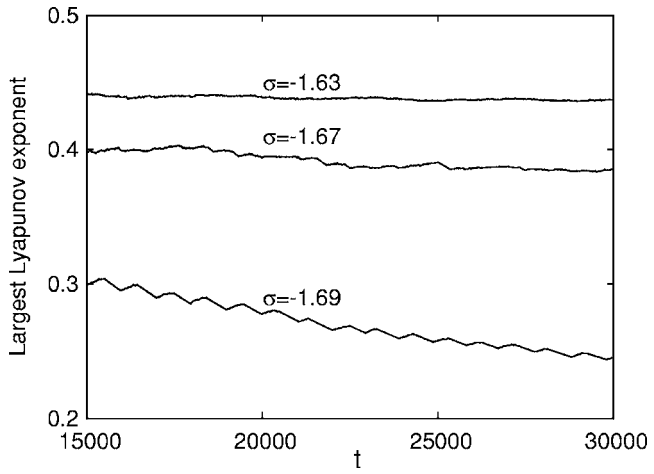

FIG. 12. Slow convergence of the largest Lyapunov exponent for orbits in the parameter region where bursting is emergent. The parameters are set at $N=32$, $g_c=0.02$, and $g_e=0$. The convergence becomes slower as σ approaches the bifurcation point.

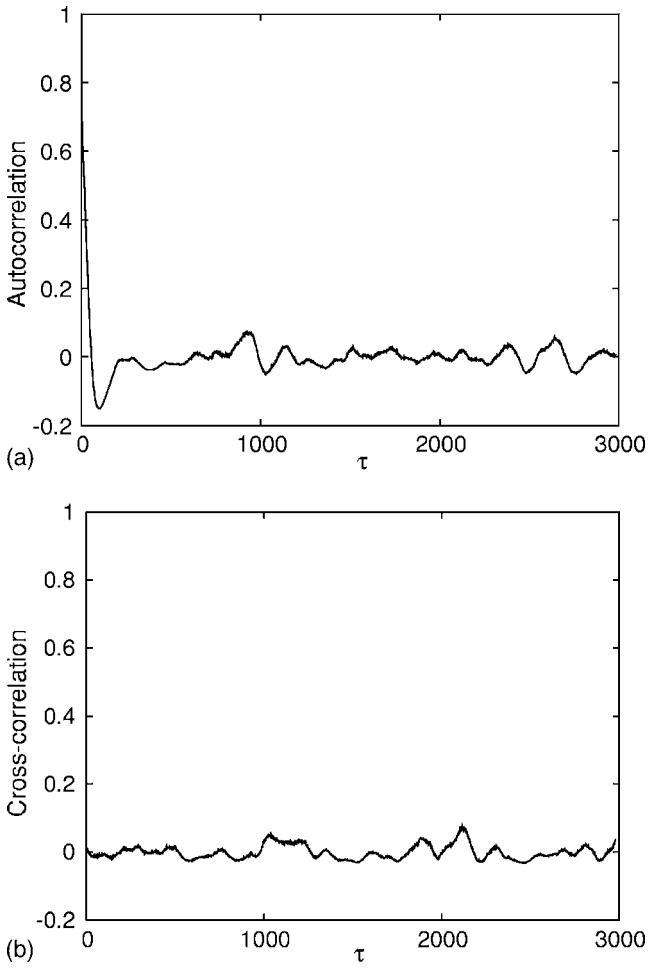

FIG. 13. Long-term sustainment of the correlations between neurons where $N=32$, $\sigma=-1.69$, $g_c=0.02$, and $g_e=0$: (a) autocorrelation of the first neuron; (b) cross-correlation between the first neuron and the 17th neuron.

The correlations do not decline exponentially but keep fluctuating over a long period of time. This characteristic implies a spatially ordered but temporally irregular structure. Therefore, an orbit exhibits history-dependent transitions in the complex patterns.

Chaotic itinerancy in coupled identical chaotic systems often corresponds to orbital motion near an invariant subspace including a Milnor attractor.[26] Although we have not proved that the ordered components of the complex itinerant patterns studied in this section are localized attractors in Milnor's sense, we have seen that they possess some characteristics of chaotic itinerancy such as the transitions among ordered global behaviors, relatively many near-zero Lyapunov exponents, the long-term persistence of correlations, and the slow convergence of the largest Lyapunov exponents.[26,32] Therefore, the complex phenomena found in the ring of map-based neurons can be considered as chaotic itinerancy analogously to the chaotic alternations between synchronized and desynchronized states and between metachronal waves in networks of ODE-based neuron models.[25]

V. CONCLUSION

We have investigated regular and complex spatiotemporal dynamics in networks of coupled map-based neurons with chaotic bursts. These networks are capable of reproducing two typical regular patterns, i.e., in-phase and antiphase synchronization of bursts. We have shown through linear stability analysis how the coupling parameters corresponding to chemical and electrical synapses determine the type of synchronous pattern. The direction in which an orbit in the vicinity of the invariant subspace is repelled and the presence of reinjection mechanism towards it determines the global dynamics. We have also focused on the complex dynamics of the network in the parameter region where bursting is emergent due to the coupling. We have demonstrated that these complex patterns are made up of chaotic transitions between nearly synchronous and propagating bursts. According to the bifurcation theory in symmetrical dynamical systems,[29] the transient ordered motions may correspond to chaotic standing and rotating waves generated by symmetry-breaking Neimark-Sacker bifurcations. Further, we have demonstrated characteristics of the complex patterns, suggesting that they can be considered as chaotic itinerancy.

The networks we have used may be seen as oversimplified due to the constraints imposed to make them amenable to general analytic treatment. Some studies consider heterogeneous neural networks with more general coupling and reproduce more realistic irregular behaviors. However, even the homogeneous network with symmetrical combined coupling studied in this paper can exhibit complex spatiotemporal patterns due to the chaotic dynamics inherent in the individual map-based neurons and thanks to symmetry-breaking bifurcations. Therefore, it is still an important problem to clarify whether the complexity of the spatiotemporal patterns exhibited by neuronal populations is due to irregularity of the individual neurons or heterogeneity and asymmetry of neural networks. Another interesting problem is the development of a theory on pattern formation through symmetry-breaking Neimark-Sacker bifurcations with their normal forms.

ACKNOWLEDGMENTS

This study has been partially supported by Grant-in-Aid for Scientific Research on Priority Areas 17022012 from The Ministry of Education, Culture, Sports, Science and Technology of Japan. This work has been partially supported by the Spanish Ministry of Science and Technology under Project Number BFM2003-03081.

[1] J. E. Lisman, Trends Neurosci. **20**, 38 (1997).
[2] R. S. K. Wong and D. A. Prince, J. Neurophysiol. **45**, 86 (1981).
[3] M. Deschênes, J. P. Roy, and M. Steriade, Brain Res. **239**, 289 (1982).
[4] A. Szücs, R. D. Pinto, M. I. Rabinovich, and H. D. I. Abarbanel, J. Neurophysiol. **89**, 1363 (2002).
[5] P. M. Dean and E. K. Matthews, J. Physiol. (London) **210**, 255 (1970).
[6] R. M. Harris, E. Marder, and A. I. Selverston, *Dynamic Biological Networks* (MIT Press, Cambridge, 1992).
[7] N. F. Rulkov, Phys. Rev. Lett. **86**, 183 (2001).
[8] N. F. Rulkov, Phys. Rev. E **65**, 041922 (2002).
[9] E. M. Izhikevich and F. C. Hoppensteadt, Int. J. Bifurcation Chaos Appl. Sci. Eng. **14**, 3847 (2004).
[10] N. F. Rulkov, I. Timofeev, and M. Bazhenov, J. Comput. Neurosci. **17**, 203 (2004).
[11] B. Cazelles, M. Courbage, and M. Rabinovich, Europhys. Lett. **56**, 504 (2001).
[12] R. C. Elson, A. I. Selverston, H. D. I. Abarbanel, and M. I. Rabinovich, J. Neurophysiol. **88**, 1166 (2002).

[13]R. C. Elson, A. I. Selverston, R. Huerta, N. F. Rulkov, M. I. Rabinovich, and H. D. I. Abarbanel, Phys. Rev. Lett. **81**, 5692 (1998).
[14]A. Sherman and J. Rinzel, Proc. Natl. Acad. Sci. U.S.A. **89**, 2471 (1992).
[15]H. D. I. Abarbanel, R. Huerta, M. I. Rabinovich, N. F. Rulkov, P. F. Rowat, and A. I. Selverston, Neural Comput. **8**, 1567 (1996).
[16]P. Varona, J. J. Torres, H. D. I. Abarbanel, M. I. Rabinovich, and R. C. Elson, Neural Networks **14**, 865 (2001).
[17]M. Rabinovich, A. Volkovskii, P. Lecanda, R. Huerta, H. D. I. Abarbanel, and G. Laurent, Phys. Rev. Lett. **87**, 068102 (2001).
[18]J. M. Casado, Phys. Rev. Lett. **91**, 208102 (2003).
[19]J. J. Collins and I. Stewart, Biol. Cybern. **71**, 95 (1994).
[20]R. Huerta, M. Bazhenov, and M. I. Rabinovich, Europhys. Lett. **43**, 719 (1998).
[21]C. Fohlmeister, W. Gerstner, R. Ritz, and J. L. van Hemmen, Neural Comput. **7**, 905 (1995).
[22]A. Sherman and J. Rinzel, Biophys. J. **59**, 547 (1991).
[23]G. de Vries, Phys. Rev. E **64**, 051914 (2001).
[24]M. A. Matías, V. P.-Muñuzuri, M. N. Lorenzo, I. P. Mariño, and V. P.-Villar, Phys. Rev. Lett. **78**, 219 (1997).
[25]I. Tsuda, H. Fujii, S. Tadokoro, T. Yasuoka, and Y. Yamaguti, J. Integrative Neuroscience **3**, 159 (2004).
[26]K. Kaneko and I. Tsuda, Chaos **13**, 926 (2003).
[27]L. M. Pecora and T. L. Carroll, Phys. Rev. Lett. **80**, 2109 (1998).
[28]H. Korn and P. Faure, C. R. Biol. **326**, 787 (2003).
[29]M. Golubitsky, I. N. Stewart, and D. G. Schaeffer, *Singularities and Groups in Bifurcation Theory: Vol. II*, Vol. 69 of Applied Mathematical Sciences (Springer, New York, 1988).
[30]Y. Kuramoto, *Chemical Oscillations, Waves, and Turbulence* (Springer, New York, 1984).
[31]P. Frederickson, J. L. Kaplan, E. D. Yorke, and J. A. Yorke, J. Diff. Eqns. **49**, 185 (1983).
[32]K. Kaneko, Phys. Rev. Lett. **69**, 905 (1992).